## Quantitative Characterization of Protein-Lipid Interactions by Free Energy Simulation Between Binary Bilayers

Soohyung Park<sup>†</sup>, Min Sun Yeom<sup>‡</sup>, Olaf S. Andersen<sup>§</sup>, Richard W. Pastor<sup>¶\*</sup>, and Wonpil Im<sup>†§\*</sup>

†Departments of Biological Sciences and Bioengineering, Lehigh University, Bethlehem 18015, Pennsylvania; ‡Korean Institute of Science and Technology Information, Daejeon, Korea; Department of Physiology and Biophysics, Weill Cornell Medicine, New York, New York 10065, United States; Laboratory of Computational Biology, National Heart, Lung and Blood Institute, National Institutes of Health, Bethesda, Maryland 20892, United States; School of Computational Sciences, Korea Institute for Advanced Study, Seoul 02455, Republic of Korea

\*Corresponding Authors: wonpil@lehigh.edu and pastorr@nhlbi.nih.gov

#### **ABSTRACT**

Using a recently developed binary bilayer system (BBS) consisting of two patches of laterally contacting bilayers, umbrella sampling molecular dynamics (MD) simulations were performed for quantitative characterization of protein-lipid interactions. The BBS is composed of 1,2-dilauroylsn-glycero-3-phosphocholine (DLPC) and 1,2-dimyristoyl-sn-glycero-3-phosphocholine (DMPC) with an embedded model membrane protein, a gramicidin A (gA) channel. The calculated free energy difference for the transfer of a gA channel from DLPC (hydrophobic thickness  $\approx 21.5 \text{ Å}$ ) to DMPC (hydrophobic thickness  $\approx 25.5$  Å) bilayers,  $\Delta G(DLPC \rightarrow DMPC)$ , is  $-2.2 \pm 0.7$  kcal/mol. This value appears at odds with the traditional view that the hydrophobic length of the gA channel is ~22 Å. To understand this discrepancy, we first note that recent MD simulations by different groups have shown that lipid bilayer thickness profiles in the vicinity of a gA channel differ qualitatively from the traditional deformation profile predicted from continuum elastic bilayer models. Our MD simulations at low and high gA:lipid molar ratios and different membrane compositions indicate that the gA channel's effective hydrophobic length is ~26 Å. Using this effective hydrophobic length,  $\Delta G(DLPC \rightarrow DMPC)$  determined here is in excellent agreement with predictions based on continuum elastic models (-3.0 to -2.2 kcal/mol) where the bilayer deformation energy is approximated as a harmonic function of the mismatch between the channel's effective hydrophobic length and the hydrophobic thickness of the bilayer. The free energy profile for gA in the BBS includes a barrier at the interface between the two bilayers which can be attributed to the line tension at the interface between two bilayers with different hydrophobic thicknesses. This observation implies that translation of a peptide between two different regions of a cell membrane (such as between the liquid ordered and disordered phases) may include effects of a barrier at the interface in addition to the relative free energies of the species far from the interface. The BBS allows for direct transfer free energy calculations between bilayers without a need of a reference medium, such as bulk water, and thus provides an efficient simulation protocol for the quantitative characterization of protein-lipid interactions at all-atom resolution.

#### **KEYWORDS**

Hydrophobic match; Bilayer deformation; Umbrella sampling; Line tension

#### I. Introduction

The bilayer regulation of membrane protein function and sorting is often explained using a model wherein protein-lipid interactions are optimized to match the hydrophobic length l of the protein's transmembrane domain and the hydrophobic thickness  $d_{\rm H}$  of the lipid bilayer.<sup>1,2</sup> Depending on the mismatch between l and  $d_{\rm H}$ , either protein or lipids, or both may adapt to the mismatch (**Fig. 1**); i.e., proteins may tilt or adjust their structures and lipids may stretch or compress in order to minimize the local mismatch. Unfortunately, it remains difficult to quantitatively characterize protein-lipid interactions (even in computational studies). Consequently, there is little information about how much and why protein function and stability differ among bilayers, and to what extent protein-lipid interactions and bilayer deformation penalties caused by inclusion of the protein contribute to the observed differences in function and stability.<sup>3,4</sup>

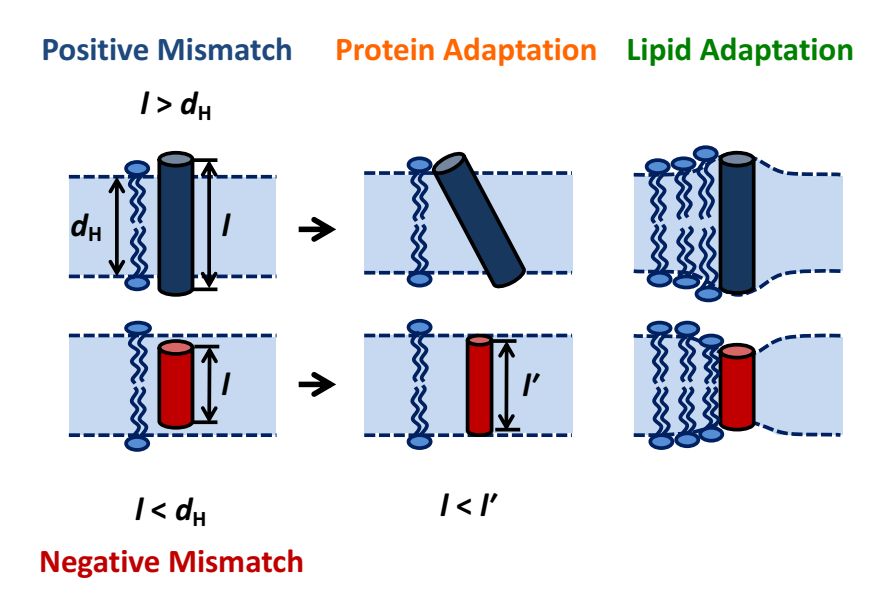


**Figure 1.** Schematic representation of possible protein-lipid interactions in the presence of a hydrophobic mismatch. While lipid adaptation is a more likely option in the negative mismatch, the embedded protein could partially unfold or stretch/thin to match its hydrophobic length to the hydrophobic thickness of membrane. Protein expulsion from the membrane is not considered here.

There have been numerous efforts to quantitatively characterize protein-lipid interactions, <sup>5–12</sup> usually by calculating a membrane protein's insertion free energy from bulk water into the membrane. <sup>5–9</sup> Using this strategy, one would need to perform two sets of insertion free energy simulations to calculate the relative free energy of a membrane protein in two different membranes. This is expensive and prone to errors resulting from the separately estimated insertion free energies or even impossible for a large membrane protein. These issues can be avoided if one could calculate the transfer free energy of a membrane protein directly between two bilayers. Recently, we designed a binary bilayer system (BBS) consisting of two patches of laterally contacting bilayers that allows for direct estimates of the partitioning of embedded molecules between different bilayers. <sup>13</sup> As an illustrative case, the partition coefficient of cholesterol between the two

different bilayers was then obtained by allowing transfer of cholesterol between the bilayers without the need for an intermediate reference medium (e.g., bulk water).

In this study, we show that the BBS provides an effective simulation protocol for quantitative characterization of protein-lipid interactions by calculating the potential of mean force (PMF) for moving an embedded transmembrane protein between two bilayers using umbrella sampling (US).<sup>14</sup> We used the monovalent cation channel gramicidin A (gA)<sup>15</sup> as a model membrane protein in a BBS composed of 1,2-dilauroyl-*sn*-glycero-3-phosphocholine (DLPC) and 1,2-dimyristoyl-*sn*-glycero-3-phosphocholine (DMPC) bilayers. Though small, the gA channel provides a good model for protein-lipid interactions<sup>16–18</sup> due to: its structural feature shared with ion channels;<sup>19,20</sup> its anchoring Trp residues at the membrane interfaces;<sup>21,22</sup> and, critically, lipid adaptations to minimize energetic penalty arising from *l*-*d*<sub>H</sub> mismatch<sup>23,24</sup> that would be a general scenario for regulation of interactions between larger proteins and lipids.

In the scenario of lipid adaptation, the energetic penalty upon the insertion of the protein has been attributed to bilayer deformation energy in the framework of the continuum elastic models (CEMs), $^{25-29}$  which inevitably simplify the complicated protein-lipid interactions near the protein. $^{24,30,31}$  This incompleteness may make l an adjustable parameter rather than one determined from the structure. In this work, this question was also examined by comparing the relative free energy from the US simulations and that from the CEM with a traditionally accepted gA channel's l of 22 Å. $^{23,32}$  To determine a most likely value of l in the framework of the CEM, extensive molecular dynamics (MD) simulations were also performed.

The paper is organized as follows. In the next section (Sec. II), the BBS system set up for US simulation and bilayer MD simulations and computational methods are described. In Sec. III, the general behavior of the BBS used in the US simulations is presented, which is followed by the results from US simulations. Sec. IV shows the results from MD simulations matching the earlier experimental work for the determination of gA channel's l. Sec. V begins with further analysis and validation of the BBS followed by a discussion of the disagreement between the PMF-derived relative free energy and CEM-based predictions. We introduce the (protein centric) molecular l (l<sub>mol</sub>) and the (bilayer centric) effective l (l<sub>eff</sub>) to reconcile the disagreement. The calculated free energy difference from the US simulations agree with the difference in bilayer deformation energies in two bilayer environments using a l<sub>eff</sub> of 26 Å. A simple model including line tension is proposed, which accurately describes the characteristics of the calculated free energy profile using the BBS. Concluding remarks are presented in Sec. VI.

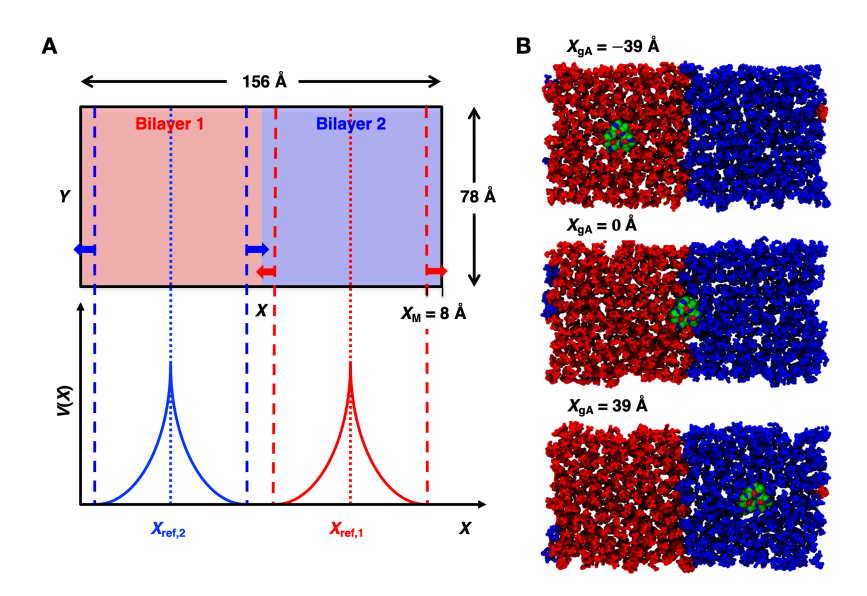


**Figure 2.** (A) (Top) A schematic of the binary bilayer system and (Bottom) the soft restraint potentials applied to each lipid. Each lipid in bilayer 1 (bilayer 2) experiences an inverted flat-bottomed harmonic restraint potential shown as red (blue) curves to prevent bilayer mixing. Vertical lines are shown for visual guidance. (B) Initial configurations for umbrella sampling simulations (top view). The *X* center of mass of the gA channel (spheres) is at  $X_{gA} = -39 \text{ Å}$ , 0 Å, and 39 Å. DLPC (red) and DMPC (blue) are shown as sticks. Hydrogen atoms, ions, and water are omitted for clarity.

#### II. Methods

#### Molecular dynamics simulations of gA in DLPC/DMPC binary bilayer

For the PMF calculations along the X center of mass of an embedded gA channel ( $X_{gA}$ ), an umbrella sampling (US) simulation system along  $X_{gA}$  in a BBS of two pure lipid bilayers of DLPC and DMPC was prepared. The initial XY dimensions of each BBS window were set to be  $L_X = 156$  Å and  $L_Y = 78$  Å<sup>2</sup> ( $L_X = 2L_Y$ ) to incorporate at least three lipid shells around gA (**Fig. 2**),<sup>30,31</sup> where  $L_X$  and  $L_Y$  are the system size along the X and Y dimensions, respectively. Each BBS window was composed of 180 DLPC and 180 DMPC lipids with an embedded gA (PDB ID: 1JNO)<sup>33</sup> at a given target  $X_{gA}$ , bulk water, and 0.15 M KCl. The target values of  $X_{gA}$  for the windows were uniformly distributed along the X direction with a spacing d of 1 Å in a range of [–54 Å, 54 Å], where X = 0 Å is the X center of the simulation box. The associated bias force constant X was set to be 3.6 kcal/(mol·Å<sup>2</sup>), an optimal value obtained from the relation,  $X_{gA}$  and  $X_{gA}$  distributions from the all pairs of windows separation of  $X_{gA}$  in the preliminary replica exchange US for a windows separated by 1 Å in the preliminary replica exchange US simulations (data not shown).

Each BBS window was prepared and equilibrated by following a six-step protocol employed in CHARMM-GUI *Membrane Builder*,  $^{35-38}$  where modifications were made to initially locate DLPC and DMPC lipids at X < 0 Å and X > 0 Å, respectively. To prevent bilayer mixing, soft restraint potentials were applied to the phosphorous atoms of all lipids (**Fig. 2**), which acts once a lipid in

a bilayer diffused into the other bilayer deeper than a pre-defined limit  $X_{\rm M}$  from the bilayer-bilayer interfaces at  $X \approx 0$  Å ( $X_{\rm M} = 8$  Å in the present study). An inverted flat-bottomed harmonic restraint potential was used for the binary bilayer restraining potential, V(X),

$$V(X) = \begin{cases} k_{\rm r}(r - d_{\rm r})^2 / 2 & (r - d_{\rm r} < 0) \\ 0 & (r - d_{\rm r} \ge 0) \end{cases}$$
 (1)

where the force constant  $k_r$  was set to 0.5 kcal/(mol·Å<sup>2</sup>),  $r = |X - X_{ref}|$ , and  $d_r = L_X/4 - X_M$ , and  $X_{ref}$  for lipids in DLPC and DMPC bilayer were set to  $L_X/4$  and  $-L_X/4$ , respectively.<sup>13</sup>

For the prepared windows, a series of short constant volume and temperature (NVT) and constant pressure and temperature (NPT) equilibration runs were performed, during which various restraint potentials were gradually relaxed to vanish except the umbrella and binary bilayer restraining potentials (kept throughout the whole simulation). A 360-ns NPT production run was performed for each window at p=1 bar and T=303.15 K. The  $X_{\text{ref}}$  and target  $X_{\text{gA}}$  for all windows were updated every 1 ns using the instantaneous box sizes.

## Molecular dynamics simulations of gA in homogeneous bilayers matching experiments

To resolve the origin of the difference between the hydrophobic length of the gA channel deduced in previous experimental studies<sup>23,32</sup> ( $l_{\text{mol}}$ ) and that of the current results ( $l_{\text{eff}}$ ), we begin by noting that the recent simulation studies<sup>24,30,31,39,40</sup> all show that the bilayer thickness profile near the channel is much more complicated than that envisaged in the earlier CEM studies.<sup>27,28,41–43</sup> We therefore built and simulated various molecular systems matching the earlier experimental work: a gA channel embedded in a monopalmitolein (MPLO) bilayer—in the absence (gA:MPLO)<sup>32</sup> and presence of n-decane (gA:MPLO:NDEC)—and that in DLPC and DMPC bilayers (gA:DLPC and gA:DMPC, respectively) at a gA:lipid molar ratio of 1:10 (similar to the experiments of Harroun et al.<sup>23</sup>).

For gA:MPLO systems, two different gA:MPLO molar ratios, 1:20 and 1:160, were considered. Each simulation system was prepared first by generating corresponding palmitoleic acid (PALO) bilayer with an embedded gA channel using *Membrane Builder*<sup>35–38</sup> followed by replacement of PALO molecules with MPLO molecules while keeping the number of other components. The prepared simulation system consisted of a gA channel, bulk water with 0.15 M KCl, and 40 and 320 MPLO molecules at the molar ratio of 1:20 and 1:160, respectively. For gA:MPLO:NDEC systems, two gA:MPLO:NDEC molar ratios, 1:10:10 and 1:80:80, were considered. Each simulation system was prepared by following the same procedure for the preparation of the gA:MPLO systems. For gA:DLPC and gA:DMPC systems, each simulation system was prepared using *Membrane Builder*. Five independent replicates for each system were prepared for better statistics. The system information is listed in **Table 1**. For each replicate, a series of short NVT and NPT equilibration runs were carried out followed by a 200-ns NPT production run at p = 1 bar and at two temperatures T = 296.15 K and T = 303.15 K except gA:DMPC systems that were simulated only at T = 303.15 K.

**Table 1**. System information for a gA in homogenous bilayers matching experiments.

System	Composition <sup>a</sup>	Ions	Initial size (Å <sup>3</sup> )
gA:DLPC	1:10	None	$30 \times 30 \times 79$
gA:DMPC	1:10	None	$30 \times 30 \times 79$
gA:MPLO	1:20	0.15 M KCl	$30 \times 30 \times 85$
	1:160	0.15 M KCl	$71 \times 71 \times 85$
gA:MPLO:NDEC	1:10:10	0.15 M KCl	$30 \times 30 \times 85$
	1:80:80	0.15 M KCl	$71 \times 71 \times 85$

<sup>&</sup>lt;sup>a</sup>Molar ratio of gA monomer and other components. There is a single gA channel (dimer) in the system.

## Simulation protocol

All simulations were performed by using OpenMM<sup>44</sup> with the C36 protein<sup>45</sup> and lipid<sup>46</sup> force fields and TIP3P water model;<sup>47–49</sup> the force field parameter for MPLO were transferred from those of PALO (for hydrocarbon tail) and di-palmitoleic-phosphatidylglycerol (for glycerol head group). The integration time step was set to 2 fs with SHAKE algorithm<sup>50</sup> for constraining covalent bonds involving hydrogen atoms. The van der Waals interactions were smoothly switched off over 10–12 Å by a force-based switching function<sup>51</sup> and the electrostatic interactions were calculated by particle-mesh Ewald method.<sup>52</sup> The temperature and the pressure was controlled by Langevin dynamics with a friction coefficient 1 ps<sup>-1</sup> and a semi-isotropic Monte Carlo barostat<sup>53,54</sup> with a pressure coupling frequency of 100 steps. For MD simulations of a gA in homogeneous bilayers, the scripts from CHARMM-GUI were used.<sup>55</sup> For US simulations of a gA in DLPC/DMPC binary bilayer, these scripts were modified, where V(X) and the umbrella potential for the gA were calculated by using CustomExternalForce class in OpenMM.<sup>44</sup>

#### **Analysis**

To analyze the orientations and the insertion depth of gA, two gA monomer helices defined by  $C\alpha$  atoms of the gA channel were used. The average tilt angle of two gA monomers with respect to the membrane normal (the Z axis) and the average Z center of mass (Z-COM) were calculated. The molecular hydrophobic length of the gA channel,  $l_{mol}$ , was calculated as the distance between the centers of two circles defined by the nitrogen atoms in the indole group in Trp residues (W11, W13, and W15) in each gA monomer.

For spatially resolved analysis of lipid adaptation along the XY plane (see **Table 2**), a (two-dimensional) Voronoi tessellation approach was employed,<sup>31</sup> where we represented the gA by the C $\alpha$  atoms, and DLPC, DMPC, and MPLO molecules by the COM of acyl chain(s). We did not consider n-decane (NDEC) molecules because they were buried between MPLO layers. Voronoi tessellation in the XY plane was performed for both leaflets for each frame in a given trajectory.

For the calculation of the bilayer hydrophobic thickness,  $d_H$ , the Z position of each lipid was represented by the average Z position of the first carbon atoms in sn-1 and sn-2 tails for DLPC and DMPC, and the Z position of the first acyl-chain carbon atom for MPLO. Similarly to Pandit et al., <sup>56</sup> transbilayer nearest neighbor lipid pairs were assigned—for a lipid in a given leaflet, the laterally nearest lipid in the opposite leaflet was assigned as its transbilayer nearest neighbor. Then,  $d_H$  at the XY-COM of the pair was calculated as the Z distance between the pair of lipids. From the

calculated  $d_{\rm H}$  for the pairs, two-dimensional and radial  $d_{\rm H}$  profiles,  $d_{\rm H}$  (X, Y) and  $d_{\rm H}$  (R), were calculated, where R is the distance between the XY-COMs of the gA channel and the transbilayer nearest neighbor pair.

**Table 2**. List of thicknesses

Symbol	Meaning
l	gA channel's hydrophobic length
<i>l'</i>	gA channel's hydrophobic length adapted to a bilayer
$l_{ m mol}$	gA channel's molecular hydrophobic length (protein centric)
$l_{ m eff}$	gA channel's effective hydrophobic length (bilayer centric)
$d_{ m H}$	Hydrophobic thickness of a bilayer (at equilibrium)
$d_{ m B}$	Bilayer thickness (head group to head group)

For the calculation of bilayer thickness,  $d_B$ , we represent each lipid by the COM of phosphate group for DLPC and DMPC and by the COM of oxygen atoms in glycerol head group for MPLO, respectively. Then, similar to  $d_H$  calculation, the Z distance between lipids in the transbilayer nearest neighbor pair was assigned as  $d_B$  at the XY-COM of the pair. The radial  $d_B$  profile and shell average  $d_B$  were then calculated by using the same protocol for  $d_H$  calculations.

The radial distribution function, g(R), were calculated for the lipid tail and head group COMs by  $g(R) = (N(R+dR)-N(R))/(2\pi RdR \ \rho_{\text{bulk}})$ , where N(R) is the number of lipids within a radius R from the XY-COM of gA and  $\rho_{\text{bulk}}$  is the bulk density of the lipid in the XY dimensions.

In the analysis of the lipid adaptation at different shells, lipid shells in a given leaflet were determined rather simply based on the contacts between Voronoi cells. Similar to the work of Beaven et al,<sup>31</sup> the first shell lipids were identified as those contacting the gA, and the second shell lipids were identified as the lipids contacting the first shell lipids but not the gA. This procedure was repeated until all lipid molecules were assigned to their appropriate lipid shell. Using the assigned lipids in each lipid shell, the shell-average  $d_{\rm H}$  was calculated. Shell-average deuterium order parameter  $S_{\rm CD} = |<(3\cos^2\theta - 1)/2>|$  was also calculated from those for each acyl chain, where  $\theta$  is the angle between C-H bond and the bilayer normal (the Z axis).

## III. Results from umbrella sampling simulations of gA in DLPC/DMPC binary bilayer

Here, we present the results from the US simulations of gA in DLPC/DMPC binary bilayer. First, the general behavior of BBS is described and the PMF is presented. Then, the adaptations between gA and bilayers are examined.

## Binary bilayer system behavior

To check the self-adjusted lipid packing of the BBS windows and the interfaces between DLPC and DMPC bilayers, we examined the system size ( $L_X$  and  $L_Y$ ), the number of lipids under the restraints ( $N_{res}$ ) and those under the restraints above the thermally accessible energy,  $2k_BT$ ,  $^{34}$  ( $N_{h-res}$ ), the applied restraining energy to BBS ( $E_{res}$ ), and the number of contacting lipids to gA ( $N_{cont}$ ).

The system size of BBS windows along the X and Y dimensions were  $L_X = 149.8 \pm 0.3$  Å and  $L_Y = 74.9 \pm 0.2$  Å, which were well maintained throughout the simulation time. In the BBS windows, about three lipid molecules in each bilayer were subject to non-vanishing V(X) ( $N_{\rm res} \approx 3.63$  and  $\approx 3.31$  for DLPC and DMPC bilayers, respectively) (**Fig. 3A**). Only a tiny fraction of lipid molecules (0.1%) were subject to the high V(X) ( $> 2k_{\rm B}T$ ) ( $N_{\rm h-res} \approx 0.17$  and  $\approx 0.15$  for DLPC and DMPC bilayers, respectively) (**Fig. 3A**), indicating no meaningful alteration of bilayer properties such as lipid packing. The rest of the restrained lipids were subject to  $V(X) < 2k_{\rm B}T$ , which can be easily overcome by thermal fluctuation. The average restraining energy applied to BBS windows ( $E_{\rm res}$ ) was also calculated (**Fig. 3B**); it was about 1.2 kcal/mol both for DLPC and DMPC bilayers. There were about 9.4 lipids in direct contact with each subunit in the gA channel ( $N_{\rm cont} = 9.39 \pm 0.01$ ), which agrees well with the number of lipid molecules in the first shell of gA in the previous MD study (9.2 ± 0.1 and 9.4 ± 0.2 for DLPC and DMPC bilayers). The  $N_{\rm cont}$  profiles for each lipid type are flat near the center of each bilayer and change rather linearly from  $N_{\rm gA} \approx -20$  Å to  $N_{\rm gA} \approx -20$  Å to  $N_{\rm gA} \approx -20$  Å (**Fig. 3C**). Together with  $N_{\rm res}$  (and  $N_{\rm h-res}$ ),  $N_{\rm cont}$  profiles indicate that the interfaces between DLPC and DMPC bilayer were well maintained and minimally perturbed in our simulations.

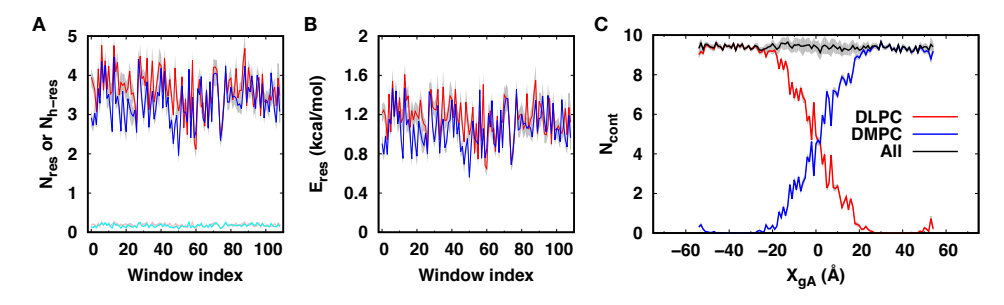


**Figure 3**. (A) Number of lipids subject to the restraint potentials ( $N_{\text{res}}$ ) and those subject to the high restraint potential above the thermally accessible energy,  $2k_{\text{B}}T$ , ( $N_{\text{h-res}}$ ) calculated from 20-ns block averages for all windows.  $N_{\text{res}}$  and  $N_{\text{h-res}}$  for DLPC bilayer are shown in red and pink, and those for DMPC bilayers are shown in blue and cyan, respectively. Note that the pink and cyan lines are almost identical. (B) The average binary bilayer restraining energy,  $E_{\text{res}}$ , applied to each bilayer in the BBS windows calculated from 20-ns block averages. (C) The number of contacting lipids to gA,  $N_{\text{cont}}$ , as a function of  $X_{\text{gA}}$ . The standard errors over the block averages are depicted by the gray area.

## Free energy profile

The PMF along  $X_{\rm gA}$  was obtained from the last 300-ns trajectories using 20-ns block PMFs calculated by WHAM. The PMF profile (**Fig. 4**) shows plateaus in both the DLPC and the DMPC bilayer sides. These plateaus are symmetric with respect to their centers ( $X_{\rm gA} \approx -39$  Å and  $X_{\rm gA} \approx 39$  Å, respectively) whose half-width  $W_X$  is 7-8 Å. Considering the geometry of the BBS, the DLPC bilayer (in the primary simulation box) are surrounded by two equivalent DMPC bilayers along  $X_{\rm gA}$  (i.e., one is in the primary simulation box and the other is its image). Similarly, the DMPC bilayers are surrounded by two equivalent DLPC bilayers. Therefore, there should be two mirror symmetries in the PMF profile at the centers of DLPC and DMPC bilayers along  $X_{\rm gA}$ . The observed mirror symmetries in the PMF profile thus indicate that our US binary bilayer simulations were valid. The transfer free energy of a gA channel from a DLPC to a DMPC bilayer,

 $\Delta G(DLPC \rightarrow DMPC)$ , was estimated as the difference between the two plateaus centered at -39 Å and 39 Å, respectively:  $\Delta G(DLPC \rightarrow DMPC) = -2.2 \pm 0.7$  kcal/mol. Between two plateaus, there is a barrier of  $\sim 1.3$  kcal/mol relative to the DLPC side and  $\sim 3.5$  kcal/mol relative to the DMPC side.

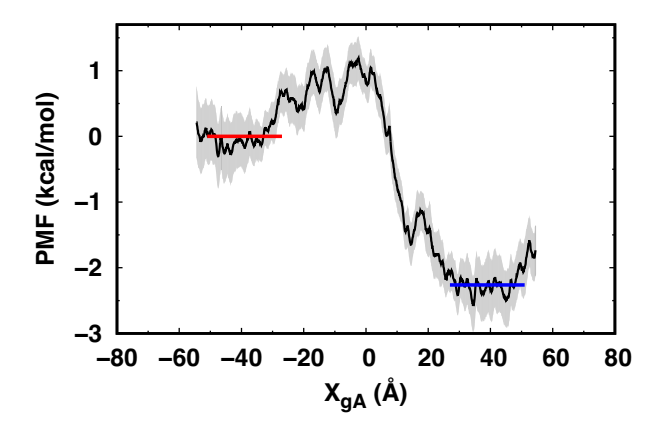


**Figure 4.** The potential of mean force (PMF) of a gA channel as function of  $X_{\rm gA}$  calculated from the last 300-ns of the umbrella sampling.  $\Delta G({\rm DLPC} \rightarrow {\rm DMPC}) = -2.2 \pm 0.7$  kcal/mol was estimated by subtracting the average PMF of two plateaus centered at  $X_{\rm gA} = -39$  Å (DMPC) and  $X_{\rm gA} = 39$  Å (DLPC) with the width  $W_X$  of 8 Å. The standard errors from 20-ns block PMFs are shown in grey.

## gA and lipid adaptations

To evaluate the general behavior of the adaptation between the channel and the bilayers, we examined the tilt angle of the gA dimer, the variation in  $d_{\rm H}$  within the BBS windows, and the interactions between the gA residues and their environments.

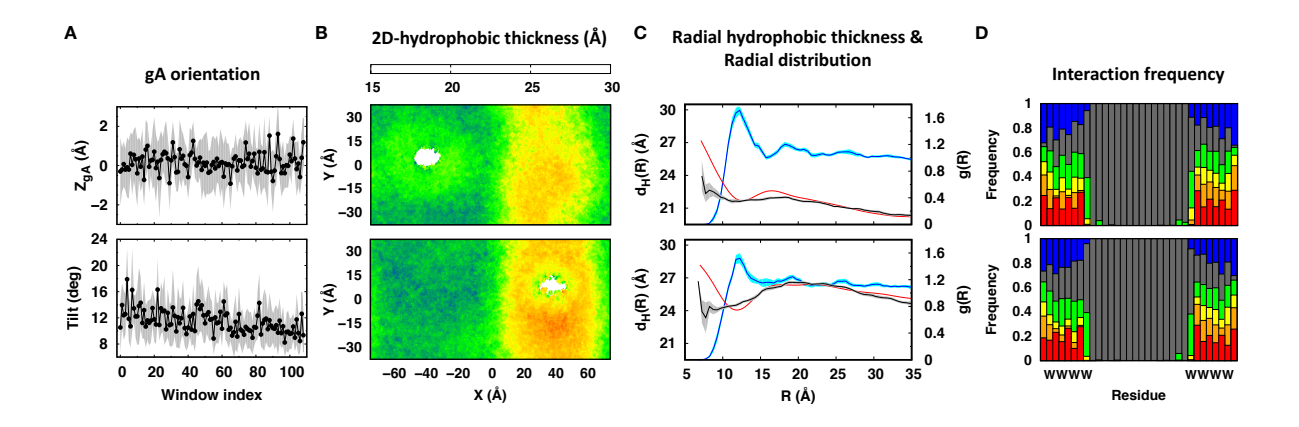


**Figure 5.** (A) The Z-COM ( $Z_{gA}$ ) and tilt angle of the gA channel. The gray areas represent one standard deviation. (B) Two-dimensional bilayer hydrophobic thickness profile,  $d_H(X,Y)$ , at  $X_{gA} = -39$  Å or  $X_{gA} = 39$  Å. (C) Radial hydrophobic thickness profiles (black line),  $d_H(R)$ , around gA at

 $X_{\rm gA} = -39$  Å (top) or  $X_{\rm gA} = 39$  Å (bottom), overlaid with those from Ref. 30 (red lines), and radial distribution function, g(R), of the lipids (blue). The gray area represents an envelope of  $d_{\rm H}(R)$  defined by the minimum and maximum values of  $d_{\rm H}$  at each R from 20-ns block averages. The cyan area represents one standard error over 20-ns block averages of g(R). The bin size along the X and Y directions is set to 0.5 Å for the calculation of the  $d_{\rm H}$  profiles. (D) Interaction patterns of gA residues with the neighboring environments at  $X_{\rm gA} = -39$  Å (top) or  $X_{\rm gA} = 39$  Å (bottom). For each residue, the frequency of occurrence of interaction partners within 4 Å were calculated (except for pore water molecules between the two gA Trp15 residues along the membrane normal). The interaction partners are labeled as follows: water (blue), choline (red), phosphate (orange), glycerol backbone (yellow), carbonyl (green), and hydrocarbon tail (gray) groups. The outer most residues are the C-terminal ethanolamides. For clarity, only Trp residues are shown in the label.

As shown in **Fig. 5A**, the insertion depth of the gA channel did not vary significantly along  $X_{\rm gA}$ . In addition, in contrast to single-pass transmembrane helices that favor tilting to minimize hydrophobic mismatch,  $^{11,30,57}$  the tilt of the gA channel decreased only slightly from  $\sim 12^{\circ}$  in DLPC to  $\sim 10^{\circ}$  in DMPC. This is due to the anchoring Trp residues which hydrogen bond to lipids<sup>22</sup> and thus limit tilt of the gA channel. In the two-dimensional  $d_{\rm H}$  profile,  $d_{\rm H}(X,Y)$  (**Fig. 5B**),  $d_{\rm H}$  around the gA channel deviated from its bulk toward  $d_{\rm H} \sim 24$  Å for both DLPC and DMPC bilayers, indicating the lipid adaptation to minimize the energetic penalty due to the mismatch in the bulk  $d_{\rm H}$  and l of the gA channel. The perturbation in  $d_{\rm H}(X,Y)$  extends 25–30 Å radially from the XY-COM of gA and approaches to the bulk  $d_{\rm H}$  at larger distances. At the bilayer-bilayer interfaces (X = 0 Å), the value of  $d_{\rm H}$  becomes the average of those for DLPC and DMPC bilayers.

The difference in the lipid adaptation between DLPC and DMPC bilayer are also clearly shown in the radial hydrophobic thickness profiles  $d_{\rm H}(R)$  (**Fig. 5C**), which show excellent agreement with those from the previous simulation study in individual pure bilayers<sup>30</sup> except the vicinity of the gA channel (R < 10 Å). We attribute the rather large differences in  $d_{\rm H}(R)$  at R < 10 Å between the present and previous work to the difference in defining  $d_{\rm H}$  at R. (Better agreement with previous work was obtained when  $d_{\rm H}$  was calculated as the difference between leaflet hydrophobic thicknesses, data not shown.) The larger uncertainties in  $d_{\rm H}(R)$  at R < 10 Å reflects the complex lipid packing adjacent to the gA channel such as protrusion of the lipids up over the channel as well as the small number of such lipids, N(R = 10 Å) ( $0.4 \pm 0.1$  for DLPC and  $0.5 \pm 0.1$  for DMPC, respectively, obtained by the integration of g(R)). The agreement of  $d_{\rm H}(R)$  between BBS and the individual pure bilayers further validates BBS.

The gA-bilayer interfaces were not sensitive to the lipid type (**Fig. 5D**) and the interaction pattern of the amino acid residues in the channel with the neighboring environments is consistent with our previous study. The phospholipid head group interacts with the first seven residues from the C terminus (i.e., four Trp residues, and the Leu residues in-between them), but its interaction frequency with the first three Trp residues is higher than that with the Leu residues. The interactions between the first four residues (< 1 turn of  $\beta^{6.3}$ -helix<sup>58</sup>) with carbonyl groups and hydrocarbon tails are consistent with the hot spots shown previously, where the lipids protrude up over the channel so that these groups can interact with these residues. Residues beyond the fourth Trp residue have minimal interactions with the head groups. The tightly regulated gA-bilayer interfaces together with minimal gA adaptation implies that  $\Delta G(\text{DLPC}\rightarrow\text{DMPC})$  is

determined primarily by the difference in lipid adaptation (i.e., bilayer deformation free energy,  $\Delta G_{\text{def}}$ ) in the two bilayer environments, which reaches out to the third lipid shell ( $R \approx 30 \text{ Å}$ ).  $^{30,31}$ 

## IV. Simulations of gA in homogeneous bilayers matching experiments

To better understand the adaptation between gA channels and the adjacent lipid molecules, we did MD simulations of gA channels embedded in MPLO bilayers with and without NDEC, as well as single-component DLPC and DMPC bilayers at T = 303.15 K. The results of the simulation at T = 296.15 K are similar to those at T = 303.15 K.

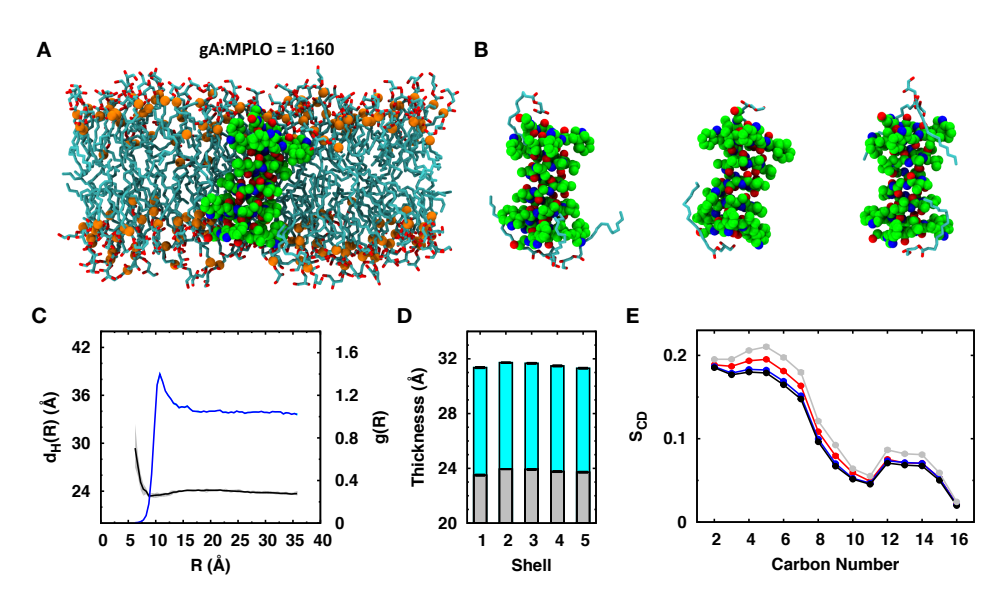


**Figure 6** (A) A final snapshot of a gA:MPLO system and (B) selected conformations of MPLO that protrude over the gA channel at a molar ratio of 1:160 at T = 303.15 K. gA is shown in spheres: C atoms (green), O atoms (red), and N atoms (blue). MPLO molecules are shown in sticks: C atoms (cyan) and O atoms (red). For visual guidance, C2 atoms in MPLO are shown as orange spheres in (A). For clarity, hydrogen atoms, water molecules, and ions are omitted. (C) Radial hydrophobic thickness ( $d_H(R)$ , black) profile and g(R) of MPLO tail's COM for gA:MPLO at the ratio of 1:160 at T = 303.15 K. The gray area represents an envelope of  $d_H(R)$  defined by their minimum and maximum values at each R from five independent simulations. The cyan area is the standard error of g(R) from five independent simulations. (D) The shell average of  $d_H$  (grey) and bilayer thickness  $d_H$  (cyan) at a molar ratio of 1:160 at T = 303.15 K. (E)  $S_{CD}$  order parameter gA:MPLO systems at molar ratio of 1:160 and 1:20 at T = 303.15 K. Shell  $S_{CD}$  for carbon atoms in the acyl chain are shown for gA:MPLO at the ratio of 1:160: the first shell (red), the second shell (blue), and the bulk (black). For gA:MPLO at the ratio 1:20,  $S_{CD}$  was calculated for the whole bilayer (grey). Standard errors were calculated over the replicas and are smaller than the size of the symbol.

The bilayer perturbations in MPLO bilayers at gA:MPLO molar ratio of 1:160 are shown in **Fig. 6A**. Similar to DLPC and DMPC bilayers, a small number of MPLO lipids ( $N(R = 10 \text{ Å}) \approx 1.4$ , calculated from the g(R) of the MPLO tail COM) that protrudes over the gA channel, where hydrogen bonds between glycerol head groups were frequently observed (**Fig. 6B**).  $d_H(R) \approx 28 \text{ Å}$ 

near the channel pore at  $R \approx 5$  Å decreases as R increases, to its minimum at  $R \approx 9$  Å (**Fig. 6C**).  $d_{\rm H}$  increases in the second shell and relaxes to its bulk value of ~24 Å beyond the third shell (**Figs. 6C** and **6D**). The  $S_{\rm CD}$  varies similarly as was the case for the DLPC tails, meaning that  $S_{\rm CD}$  becomes smaller at the second shell and approaches the bulk MPLO bilayer values (**Fig. 6E**). These results suggest a slightly positive l- $d_{\rm H}$  mismatch. Except for the first shell around the channel,  $d_{\rm B}$  is about 8 Å larger than  $d_{\rm H}$  (**Fig. 6D**). At the higher gA:MPLO ratio of 1:20, the MPLO molecules were more tightly packed as reflected in an increased  $d_{\rm H}$  for the first shell, ~0.5 Å (**Table 3**) and larger  $S_{\rm CD}$ , as compared to the results obtained at gA:MPLO = 1:160 (**Fig. 6E**). Yet,  $d_{\rm B}$  was not influenced by the tighter MPLO packing (**Table 3**).

**Table 3.** Bilayer thickness ( $d_B$ ) and hydrophobic thickness ( $d_H$ ) of the first lipid shell and the molecular hydrophobic length of the gA channel ( $l_{mol}$ ) from simulations.<sup>a</sup>

System	T(K)	$d_{\mathrm{B}}(\mathrm{\AA})$	d <sub>H</sub> (Å)	l <sub>mol</sub> (Å)
BBS $(X_{gA} = -39 \text{ Å})$	303.15	32.8 (0.1)	22.0 (0.1)	23.2 (0.1)
BBS ( $X_{gA} = 39 \text{ Å}$ )	303.15	35.4 (0.1)	25.0 (0.0)	23.3 (0.0)
gA:DLPC (1:10)	296.15	34.4 (0.2)	23.6 (0.2)	23.1 (0.0)
	303.15	34.0 (0.0)	23.3 (0.0)	23.1 (0.0)
gA:DMPC (1:10)	303.15	37.0 (0.2)	26.7 (0.1)	23.2 (0.1)
gA:MPLO (1:20)	296.15	31.4 (0.2)	24.1 (0.1)	23.1 (0.1)
	303.15	31.4 (0.1)	24.0 (0.1)	23.0 (0.1)
gA:MPLO (1:160)	296.15	31.6 (0.0)	23.7 (0.0)	23.0 (0.1)
	303.15	31.4 (0.1)	23.5 (0.1)	23.0 (0.1)
gA:MPLO:NDEC	296.15	33.1 (0.1)	26.9 (0.1)	23.1 (0.3)
(1:10:10)	303.15	33.5 (0.1)	27.3 (0.1)	23.1 (0.1)
gA:MPLO:NDEC	296.15	37.2 (0.1)	30.9 (0.1)	23.0 (0.1)
(1:80:80)	303.15	37.4 (0.3)	30.9 (0.2)	23.1 (0.3)

<sup>a</sup>Bilayer thickness,  $d_{\rm B}$ , is defined as the phosphate-to-phosphate distance (for DLPC and DMPC bilayers) and the glycerol-oxygen to glycerol-oxygen distance (for MPLO bilayers). Bilayer hydrophobic thickness,  $d_{\rm H}$ , is defined as the distance between the first acyl-chain carbon (C22 and C33) atoms. The thicknesses were calculated between the corresponding transbilayer nearest neighbor pairs. The molecular hydrophobic length of the gA channel,  $l_{\rm mol}$ , is defined as the distance between the centers of the N atoms in indole group of three Trp residues (W11, W13, and W15). The standard errors are given in parenthesis.

When a monoglyceride bilayer is formed with hydrocarbon solvent,  $d_{\rm H}$  is larger than for the corresponding pure monoglyceride bilayer.<sup>59,60</sup> In the bilayer, it has been thought that the hydrocarbon solvent molecules reside between monoglyceride monolayers and that the gA-bilayer interfaces are mainly formed by those between gA and monoglyceride molecules.<sup>28</sup> Our simulations of gA:MPLO:NDEC systems at the ratio of 1:80:80 agree well with this picture (**Fig. 7A**). Thus, the  $d_{\rm H}(R)$  profile shows characteristics of the bilayers with negative l- $d_{\rm H}$  mismatch (**Fig. 7B**).<sup>30</sup> Though the system size is too small to observe a plateau in  $d_{\rm H}(R)$ , the fourth shell  $d_{\rm H}$  of ~43 Å is in a good agreement with the previously reported  $d_{\rm H}$  of ~48 Å<sup>59</sup> (**Figs. 7B** and **7C**). At a higher

molar ratio of 1:10:10, NDEC molecules are not accumulating into the hydrophobic core due to less available space. More NDEC molecules are observed at the gA-bilayer interface (**Fig. 7A**), which is also reflected as smaller  $S_{CD}$  compared to those at the ratio of 1:80:80 (**Fig. 7D**).

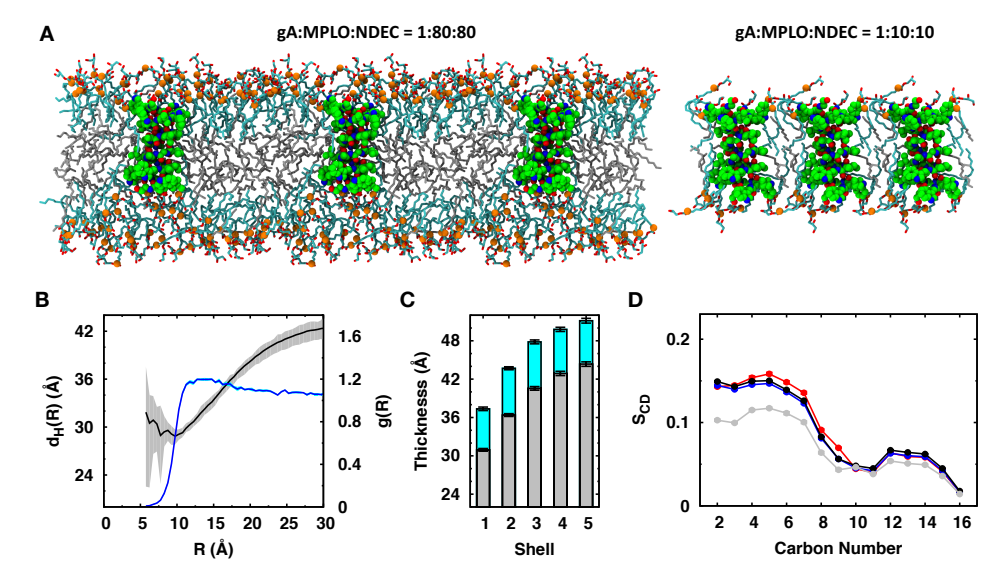


**Figure 7** (A) Snapshots of gA:MPLO:NDEC systems at gA:MPLO:NDEC molar ratios of 1:80:80 and 1:10:10 at T = 303.15 K (with two periodic images along the X direction). The color codes are the same as in **Fig. 6A** and n-decane (NDEC) molecules are shown as grey sticks. (B) Radial hydrophobic thickness  $d_H(R)$  profile and g(R) of MPLO tail COM for gA:MPLO:NDEC at the ratio of 1:80:80 at T = 303.15 K. The color codes are the same as in **Fig. 6C**. (C) The shell average of  $d_H$  (grey) and bilayer thickness  $d_B$  (cyan) at a molar ratio of 1:80:80 at T = 303.15 K. (D)  $S_{CD}$  order parameters at gA:MPLO:NDEC molar ratios of 1:80:80 and 1:10:10 at T = 303.15 K. Shell  $S_{CD}$  for carbon atoms in the acyl chain are shown for gA:MPLO:NDEC at the ratio of 1:80:80 (with the same color codes as in **Fig. 6E**). For gA:MPLO:NDEC at the ratio 1:10:10,  $S_{CD}$  was calculated for the whole bilayer (grey). Standard errors were calculated over the replicas and smaller than the size of the symbol.

The  $d_{\rm B}$  of gA:DLPC and gA:DMPC systems at gA:lipid ratio of 1:10 (**Table 3**) are larger than those reported by Harroun et al.<sup>23</sup> but similar to those from the previous molecular dynamics simulations.<sup>61,62</sup> The results are consistent with the previously reported increased order of DMPC bilayer in the presence of gA,<sup>63</sup> which is also shown as significantly larger  $S_{\rm CD}$  than pure bilayers (**Fig. 8**).

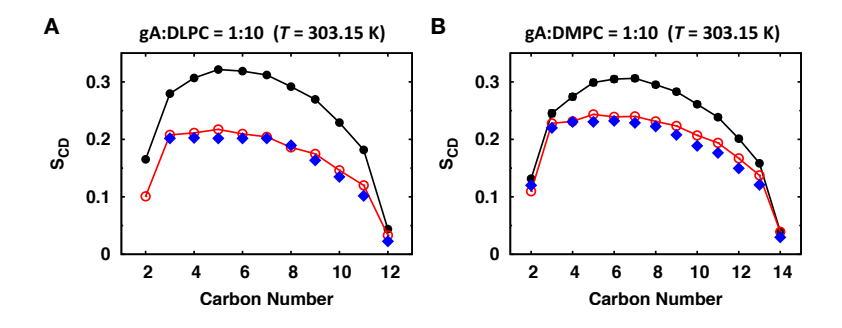


**Figure 8**.  $S_{\rm CD}$  order parameter for the gA:DLPC and gA:DMPC bilayers at a molar ratio of 1:10 at T = 303.15 K (black circle), and those for pure bilayer simulations (red circle)<sup>30</sup> and experiments (blue diamond).  $S_{\rm CD}$  for the  $S_{\rm CD}$  for the  $S_{\rm CD}$  for the  $S_{\rm CD}$  for the sm-2 tails are shown. Standard errors from the current simulations were calculated over the replicas and smaller than the size of the symbol.

#### V. Discussion

In this section, the properties of the BBS are discussed and the BBS used in the present study is validated. Then, the hydrophobic length of gA is discussed followed by a model for the gA-lipid interactions in the BBS and its implication in the translation of a membrane protein between two different regions of a cell membrane. Guidelines for a valid BBS are developed based on the free energy model and the analysis of the BBS.

#### Validation of BBS

The BBS employed in the US simulations was designed so that the laterally patched bilayers can self-adjust their packing with well-maintained interfaces while keeping the effects of V(X) being minimal. With an ideal self-adjusted lipid packing, the system dimension of the BBS can be obtained from the number of each component and its surface area as

$$L_X L_Y = 2L_Y^2 = \sum_i N_i A_i \tag{2}$$

where  $N_i$  is the number of *i*-th lipid type and  $A_i$  is its surface area in a leaflet of the BBS. For the BBS used in the present study, the system size of the BBS is obtained as  $L_Y = 75.1$  Å (=  $L_X$ /2) using  $N_{\rm DLPC} = N_{\rm DMPC} = 90$ ,  $A_{\rm DLPC} = 63.1$  Å<sup>2</sup>, and  $A_{\rm DMPC} = 60.2$  Å<sup>2</sup>, <sup>66</sup> which is in excellent agreement with the observed  $L_Y = 74.9$  Å and supports the self-adjusted lipid packing.

In addition to self-adjusted packing, for a valid BBS the interfaces between two bilayers should be well maintained. The observed  $N_{\rm res}$ ,  $N_{\rm h-res}$ ,  $E_{\rm res}$ , and  $N_{\rm cont}$  profiles (**Fig. 3**) all indicate that the interfaces between DLPC and DMPC bilayers are well maintained. To further examine whether these are controlled as designed, we compared the ratios  $N_{\rm h-res}/N_{\rm res}$  and  $E_{\rm res}/N_{\rm res}$  from the US simulations with their analytic predictions (see **Sec. A1. The analytic expressions for**  $N_{\rm res}$ ,  $N_{\rm h-res}$ , and  $E_{\rm res}$  of the BBS in the Appendix). The  $N_{\rm h-res}/N_{\rm res}$  and  $E_{\rm res}/N_{\rm res}$  from the US simulations are 0.046 and 0.32 kcal/mol for both DLPC and DMPC, which are in excellent agreement with predicted ratios,  ${\rm erfc}(2^{1/2}) = 0.046$  and  $k_{\rm B}T/2 = 0.30$  kcal/mol (Eq. A2). Also, the observed behavior that the gA farther than 20 Å from the interface between bilayers (X = 0 Å) contact only a single lipid type is consistent with the sum of the outer radius of gA (~10 Å),  $X_{\rm M}$  (~8 Å), and  $2\sigma$  (~2.2 Å). This indicates V(X) works as it is designed to prevent bilayer mixing beyond the distance  $X_{\rm M}$  from the binary bilayer interface. Together with the consistent system size with the self-adjusted lipid packing, these results validate the BBS in the present work.

#### Hydrophobic length of gA

Because the gA orientations and gA-environment interactions are not sensitive to  $d_{\rm H}$  of the DLPC and DMPC bilayers (**Fig. 5**),  $\Delta G({\rm DLPC} {\rightarrow} {\rm DMPC})$  appears to be determined primarily by the difference in the lipid adaptation (i.e., bilayer deformation free energy,  $\Delta G_{\rm def}$ ) in the two bilayer environments, which reaches up to the third lipid shell ( $R \approx 30 \text{ Å}$ ). Then,  $\Delta G({\rm DLPC} {\rightarrow} {\rm DMPC})$ 

 $\approx \Delta G_{\rm def}$ , which can be approximated in the continuum elastic models (CEMs) of lipid bilayer deformations,  $^{26-29}$  which in the simplest form reduces to

$$G_{\text{def}} = H(l - d_{\text{H}})^2 \tag{3}$$

where the force constant H is determined either theoretically<sup>26–28</sup> or experimentally.<sup>29,31</sup> The relation between lifetime and hydrophobic thickness shows that the CEM provides a good description of the gA-bilayer interactions.<sup>27,32,67</sup> In the CEM Eq. (3), H is a function of mechanical moduli<sup>41</sup> that vary little among bilayers formed by lipids with different acyl chains.<sup>68</sup> Thus, a quantitative comparison between  $\Delta G(\text{DLPC}\rightarrow\text{DMPC})$  and the difference in the deformation free energy between DLPC and DMPC bilayers,  $\Delta G_{\text{def}} = G_{\text{def}}(\text{DMPC}) - G_{\text{def}}(\text{DLPC})$ , can be made with unambiguously determined H,  $d_{\text{H}}$ , and l.

Using the experimental relation between lifetime of a gA channel and  $d_{\rm H}$ , H has been estimated to be about 50 kJ/(mol·nm²) (56 kJ/(mol·nm²)²9 and 49 kJ/(mol·nm²)³1). Theoretically, H has been estimated to be approximately 40 kJ/(mol·nm²)²6 based on analysis of the MD-derived bilayer thickness profiles, which is in reasonable agreement with the experimental estimates. The hydrophobic thicknesses of DLPC and DMPC bilayers have been determined from X-ray scattering experiments<sup>69</sup> (21.7 Å and 25.7 Å, respectively) and MD simulations<sup>66</sup> (21.2 Å and 25.3 Å, respectively), which are in excellent agreement.

The gA channel's hydrophobic length, l, was estimated by matching l to  $d_{\rm H}$  of the host bilayer in two different experimental studies: 1) a single-channel study on gA channel lifetimes in monoglyceride/squalene bilayers<sup>32</sup> and 2) X-ray scattering of gA channels embedded in DLPC or DMPC bilayers at a gA:lipid molar ratio of 1:10.<sup>23</sup> In the former experiment, a l value of about 22 Å was determined from the  $d_{\rm H}$  of the bilayer where the channel lifetime was longest. In the latter experiment, the phosphate-to-phosphate distance ( $d_{\rm B}$ ) was determined by lamellar diffraction and found to be 32.1 Å and 32.7 Å for the gA:DLPC and gA:DMPC mixture, respectively. Assuming that  $d_{\rm H}$  is 10 Å less than  $d_{\rm B}$  (as commonly assumed for pure bilayers<sup>70–72</sup>), it was concluded that l is about 22 Å, in agreement with the former experiment.

Using the CEM model in Eq.  $(3)^{29}$  and assuming  $l \approx 22$  Å, Eq. (5) predicts  $\Delta G(\text{DLPC} \rightarrow \text{DMPC}) = +1.4$  kcal/mol. This positive free energy change disagrees with the  $-2.2 \pm 0.7$  kcal/mol obtained from the PMF calculation from the US simulations (**Fig. 4**). Recent MD simulations,  $^{30,31,40,62}$  however, have shown that the lipid packing adjacent to a gA channel is more complicated than that assumed in the CEM models, and that the bilayer perturbation is larger in DLPC than in DMPC. The results to date do not, however, specify whether the complex lipid packing reflects the inherent perturbation of the membrane lipids adjacent to a membrane protein independent of channel-bilayer hydrophobic mismatch, but they raise the question what is the channel's hydrophobic length?

To pursue this question, we performed MD simulations (**Table 1**) for 1) gA channels embedded in a monopalmitolein (MPLO) bilayer at two gA:lipid molar ratios of 1:160 (similar to the conditions used by Elliott et al.<sup>32</sup>) and 1:20, 2) DLPC and DMPC bilayers at a gA:lipid molar ratio of 1:10 (similar to the conditions used by Harroun et al.<sup>23</sup>), and 3) mixed bilayers of MPLO and NDEC with an embedded gA channel at two gA:MPLO:NDEC molar ratios of 1:80:80 and 1:10:10.

The simulations imply that the channel's hydrophobic length is larger than 22 Å as judged by values of hydrophobic thickness of the first shell ( $d_{\rm H}$  in **Table 3**). However, the significant variation (22.0 to 30.9 Å) indicates that  $d_{\rm H}$  is an incomplete reflection of the channel hydrophobic length. Focusing on the channel, the hydrophobic length can be defined as the distance between the centers of the indole NH groups at Trp positions 11, 13 and 15, which is about 23 Å (**Table 3**). This value may be referred to as the (protein centric) "molecular hydrophobic length",  $l_{\rm mol}$ , which is close to 22 Å obtained earlier.

The  $l_{\rm mol}$ , however, is not necessarily directly applicable to CEM-like models, where perfect match between  $l_{\rm mol}$  and  $d_{\rm H}$  at the interfaces and smooth deformation profile are assumed. Therefore, these models cannot properly describe the complicated profile near the channel, which is seen at all bilayer thicknesses. <sup>24,30,31</sup> Hence, the lack of molecular detail in the CEM leaves l as an adjustable parameter and the notion of a hydrophobic length extracted from structure (either from experiment or simulation) is tenuous. Indeed, in the previous MD simulations, <sup>30</sup> the bilayer deformation is minimal for the DMPC ( $d_{\rm H} \approx 25.5$  Å) among bilayers formed by lipids with different acyl chains ( $d_{\rm H}^{\rm DLPC} < d_{\rm H}^{\rm DMPC} < d_{\rm H}^{\rm DOPC} \approx d_{\rm H}^{\rm POPC}$ ) and, in a recent CEM study based on MD-derived deformation profiles, <sup>26</sup> the gA channel's l of 26 Å was required to reproduce the lipid redistribution deduced from MD simulations. This hydrophobic length may be referred to as the (bilayer centric) "effective hydrophobic length" ( $l_{\rm eff}$ ), which is consistent to the bilayer perturbations from MD simulations and the CEM. Note that the CEM may contain other contributions than the hydrophobic mismatch. <sup>42</sup>

As the deformation profile (at R > 10 Å) and lipid redistribution were successfully reproduced with a  $l_{\rm eff}$  of 26 Å,  $^{37}$  it is reasonable to assign this value as the upper bound of  $l_{\rm eff}$  of the gA channel. The lower bound of the effective hydrophobic length can be estimated from the deuterium order parameter  $S_{\rm CD}$  for MPLO tails from the simulations of gA:MPLO (1:160). The shell  $S_{\rm CD}$  behave similarly to those for DLPC tails, such that  $S_{\rm CD}$  becomes smaller at the outer shell that approaches to that of a pure bilayer for a given carbon atom (**Fig. 6C**). This indicates a positive mismatch between the  $l_{\rm eff}$  and  $d_{\rm H}$ , implying that the  $l_{\rm eff}$  of a gA channel is larger than 24 Å (i.e.,  $d_{\rm H}$  of the bulk MPLO bilayer; **Fig. 6B**). This agrees with the previously reported shell-average  $S_{\rm CD}$  for DLPC and DMPC bilayers showing less bilayer perturbation in a DMPC bilayer. This result, together with our recent CEM study, and the first shell  $d_{\rm H}$  (~26 Å) of phosphatidylcholine bilayers with negative l- $d_{\rm H}$  mismatch together suggest that a  $l_{\rm eff}$  of 26 Å is more appropriate for the gA channel. With  $l_{\rm eff} = 26$  Å, we estimated  $\Delta G_{\rm def} = G_{\rm def}({\rm DMPC}) - G_{\rm def}({\rm DLPC})$ , which ranged from -3.0 to -2.2 kcal/mol (**Table 4**). The estimates agree well with  $-2.2 \pm 0.7$  kcal/mol based on the PMF profile (**Fig. 4**). Hence, it again verifies that the BBS is applicable for quantitative characterization of membrane protein-lipid interactions with all-atom details.

**Table 4.** Membrane deformation free energy from the continuum elastic model.<sup>a</sup>

H (kJ/(mol·nm²))	$d_{ m H}( m \AA)$		$G_{ m def}$ (kcal/mol)		$\Delta G_{ m def}$ (kcal/mol)
40.0 (1.6)h	DLPC	DMPC	DLPC	DMPC	2 ( (0, 2)
49.0 (1.6) <sup>b</sup>	21.2 (< 0.1) <sup>d</sup> 21.7 (0.4) <sup>e</sup>	25.3 (< 0.1) <sup>d</sup> 25.7 (0.5) <sup>e</sup>	2.70 (0.20) 2.17 (0.47)	0.06 (0.02) 0.01 (0.04)	-2.6 (0.2) -2.2 (0.5)

56 (NA) <sup>c</sup>	21.2 (< 0.1) <sup>d</sup>	25.3 (< 0.1) <sup>d</sup>	3.08 (0.13)	0.07 (0.02)	-3.0 (0.2)
	$21.7(0.4)^{e}$	25.7 (0.5) <sup>e</sup>	2.47 (0.46)	0.01 (0.04)	-2.5 (0.5)

 $^{a}G_{def}$  is given by Eq. (5). The standard errors of each parameter,  $G_{def}$ , and  $\Delta G_{def}$  are given in parenthesis.  $^{b}F_{rom}$  gA channel lifetime experiments in Ref. 31.  $^{c}F_{rom}$  gA channel lifetime experiments in Ref. 29 (errors are not reported).  $^{d}F_{rom}$  Ref. 66:  $d_{H}$  defined as the difference between the average positions of C22 and C33 atoms in two leaflets.  $^{e}F_{rom}$  Ref. 69:  $d_{H}$  defined as the difference between the average positions of C22 and C33 atoms in two leaflets.

## A model for gA-lipid interactions in the BBS

Now let us return to the PMF profile (**Fig. 4**). As the lipid adaptation extends up to the third lipid shell of a gA channel (**Figs. 5B** and **5C**), the free energy of a gA channel in a BBS (G) would include the contributions from the lipids in these shells. Depending on  $X_{\rm gA}$  along the X direction, these lipids are in various environments: those far from the interfaces between bilayers and/or those at the interface which is subject to a line tension due to the different bilayer properties ( $d_{\rm H}$ , bending and tilt moduli, and spontaneous curvature), including those subject to non-vanishing V(X) (Eq. (1)). Considering the lipids in these environments, we model the free energy comprising the contributions from the bilayer deformation ( $G_{\rm def}$ ), the line tension ( $G_{\rm int}$ ), and the restraining potential ( $G_{\rm res}$ ), i.e.,  $G = G_{\rm def} + G_{\rm int} + G_{\rm res}$  (see **Sec. A2. Detailed description of the model for gA-lipid interactions in the BBS**).

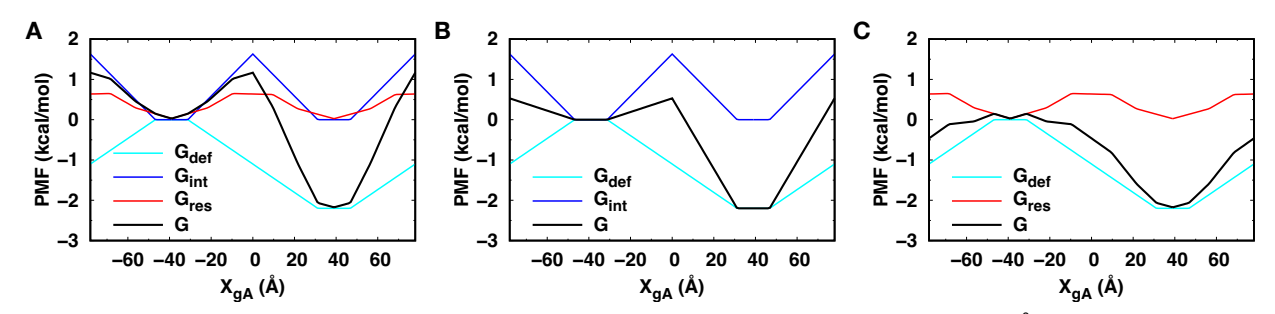


**Figure 9.** Model free energy profile (black) of gA in a BBS of DLPC (X < 0 Å) and DMPC (X > 0 Å) bilayers, where the contributions from the bilayer deformation ( $G_{def}$ , cyan), line tension ( $G_{int}$ , blue), and restraining potential ( $G_{res}$ , red) are considered fully in (A), without  $G_{res}$  in (B), and without  $G_{int}$  in (C). The free energy profile is shifted so that  $G(X_{gA} = -39 \text{ Å}) = 0 \text{ kcal/mol}$ .

The model PMF profiles are shown in **Fig. 9**, where the characteristics of the US-PMF profile (**Fig. 4**) including the width of the plateaus, the barrier at the interfaces between bilayers, and the effects of V(X) are accurately reproduced (**Fig. 9A**). While the models including the contribution from the line tension ( $G_{int}$ ) can reproduce the barrier at  $X_{gA} = 0$  Å (**Figs. 9A** and **9B**), the contribution from  $G_{res}$  alone is not sufficient for the barrier (**Fig. 9C**). Thus, we attribute the barrier at the bilayer-bilayer interface to the line tension between DLPC and DMPC bilayers. However, it should be noted that the barrier would not appear for all bilayer-bilayer interfaces. For example, the line tensions of the DOPC/DPPC and POPC/DPPC interface in our previous BBS work (at T = 318 K) were estimated using Eq. (A3) and data from recent MD simulations (at T = 298 K, 303 K, and 323 K for DOPC, POPC, and DPPC bilayers, respectively; Venable, et al., in preparation) as  $\gamma = 1000$ 

 $2.13 \times 10^{-2}$  pN and  $\gamma = 9.84 \times 10^{-3}$  pN, respectively, albeit the temperature dependence of the  $d_{\rm H}$ ,  $K_C$ , and  $K_{\theta}$  were not considered. These values are about two orders of magnitude smaller than that between DLPC and DMPC bilayers, indicating that the barrier would not be observable for the interfaces between bilayers with similar  $d_{\rm H}$ .

#### Guidelines for binary bilayer simulation

From the model of gA-lipid interactions (Sec. A2 and Fig. 9A) and theoretical consideration of the BBS, we suggest guidelines for a valid BBS for free energy simulation of membrane protein (or peptide) translation between bilayers. First, each bilayer should be sufficiently large so that the perturbed part of the bilayer arising from lipid adaptation to the protein at each bilayer center does not include the restrained lipids and line tension. For gA, each bilayer should contain at least up to the third lipid shell and the regions in which restrained lipids from the other bilayer are present. Second,  $X_{\rm M}$  for V(X) Eq (1) should be set properly for self-adjusted lipid packing. The difference in X dimension between two bilayers ( $\delta L_X$ , i.e., the shift of the X position of the interface between two bilayers from X = 0 and the others at  $X = -L_X/2$  or  $X = L_X/2$ ) can be estimated from the following relation:  $(L_X/2 + 2\delta L_X)L_Y/S_1 = (L_X/2 - 2\delta L_X)L_Y/S_2$ , as  $\delta L_X = L_X(S_1 - S_2)/(S_1 + S_2)/4$ , where  $S_1 = \sum_{i \in B_1} N_i A_i$  and  $S_2 = \sum_{j \in B_2} N_j A_j$  are the surface area of B1 and B2, respectively, and i and j are the i-th and j-th lipid types in B1 and B2. Here, it is assumed that  $S_1 > S_2$  without loss of generality. The limit  $X_{\rm M}$  should be set larger than  $\delta L_X$  for the BBS to accommodate the selfadjusted lipid packing but not too large for sharp and regular interfaces. Next,  $k_r$  should not be set too small (the distance from  $X_{\rm M}$  that a lipid may penetrate into the other bilayer is  $2^{1/2}\sigma \propto k_{\rm r}^{1/2}$ , see **Sec. A1**). When  $k_r$  is too small, a lipid in one bilayer can penetrate deep into the other bilayer. The guidelines for  $X_{\rm M}$  and  $k_{\rm r}$  for the BBS can be applied to the BBS in general purposes.

## VI. Concluding Remarks

We calculated the free energy difference of a gA channel moving from DLPC to DMPC bilayers using US simulations and the recently developed BBS (consisting of two patches of laterally contacting bilayers). The free energy profile along  $X_{\rm gA}$  shows two clear plateaus in DLPC and DMPC bilayer sides with a barrier at the DLPC-DMPC interface. The free energy difference between a gA channel in a DLPC bilayer and in a DMPC bilayer,  $\Delta G({\rm DLPC} {\rightarrow} {\rm DMPC}) = -2.2 \pm 0.7$  kcal/mol, which arises from bilayer deformations due to the tightly regulated gA-lipid interactions at the gA-lipid interfaces. This agrees well with recent MD simulation results showing that a DMPC bilayer is less perturbed than a DLPC bilayer upon the inclusion of a gA channel.

The obtained  $\Delta G(\text{DLPC}\rightarrow\text{DMPC})$  disagrees with predictions using a CEM with the conventionally accepted gA channel's l of 22 Å, which is close to (protein centric) molecular gA channel's  $l_{\text{mol}}$  of ~23 Å. Because the CEM cannot properly describe the bilayer deformation in the first lipid shell, a (bilayer centric) effective l ( $l_{\text{eff}}$ ) is introduced, which is consistent with the bilayer perturbations from MD simulations and the CEM. With a  $l_{\text{eff}} = 26$  Å, the deformation energy difference between two bilayers from the CEM (-3.0 to -2.2 kcal/mol) is in excellent agreement with the calculated free energy difference.

In addition, using a rather simple model, the characteristics of the calculated PMF profile was accurately reproduced including the widths of two plateaus, the barrier at the interfaces, and the effects of the binary bilayer restraining potentials. One important implication of the theoretical

model is that the translation of a protein or peptide in between two different regions of a cell membrane (such as between the liquid ordered and disordered phases) may include effects of a barrier at the interface.

In summary, in addition to cholesterol partitioning simulations, <sup>13</sup> the BBS can be applied to calculate partition coefficients of membrane proteins between two bilayers for quantitative characterization of protein-lipid interactions. As it allows direct transfer free energy and partition coefficient calculation of embedded components between two bilayers of any complexity without a need of a reference medium, the BBS can be an efficient and general simulation model for protein-lipid interactions with all-atom details.

## **Appendix**

In the appendix, the analytic expressions for  $N_{\text{res}}$ ,  $N_{\text{h-res}}$ , and  $E_{\text{res}}$  are derived in **Sec. A1**. Then, a model for the gA-lipid interactions in the BBS is described in detail in Sec. A2.

## A1. The analytic expressions for $N_{\text{res}}$ , $N_{\text{h-res}}$ , and $E_{\text{res}}$ of the BBS

In addition to self-adjusted packing, for a valid BBS the interfaces between two bilayers should be well maintained. Here, we derive the analytical expressions for  $N_{\text{res}}$ ,  $N_{\text{h-res}}$  and  $E_{\text{res}}$  for a BBS resulting from the binary bilayer restraining potential V(X) as follows.

Let us assume that the distribution of restrained lipids along the X direction by V(X) obeys a halfsided Gaussian distribution (defined at  $X > X_0$ ),

$$p(X) = 2/(\sqrt{2\pi}\sigma) \exp[-(X - X_0)^2/(2\sigma^2)]$$
 (A1)

where  $X_0$  is the starting position of the action of V(X) (effective at  $X > X_0$ ), and  $\sigma = (k_B T/k_r)^{1/2}$ . The p(X) is normalized over the integral from  $X_0$  to  $\infty$  and  $V(X) = k_r(X-X_0)^2/2$ . Then, the  $N_{\text{res}}$ ,  $N_{\text{h-res}}$ , and  $E_{\rm res}$  are obtained as

$$N_{\text{res}} = 2c_0 \int_{x_0}^{\infty} dX \ p(X) = 2c_0 \tag{A2a}$$

$$N_{\text{h-res}} = 2c_0 \int_{Y_{-1}/2}^{\infty} dX \, p(X) = N_{\text{res}} \text{erfc}(\sqrt{2})$$
 (A2b)

$$N_{\text{res}} = 2c_0 \int_{X_0}^{\infty} dX \ p(X) = 2c_0$$
 (A2a)  
 $N_{\text{h-res}} = 2c_0 \int_{X_0 + 2\sigma}^{\infty} dX \ p(X) = N_{\text{res}} \text{erfc}(\sqrt{2})$  (A2b)  
 $E_{\text{res}} = 2c_0 \int_{X_0}^{\infty} dX \ V(X) p(X) = N_{\text{res}} k_{\text{B}} T/2$  (A2c)

where  $c_0$  is the number density of the lipid in a bilayer along the X direction at  $X = X_0$  and  $erfc(X) \equiv$  $1 - \operatorname{erf}(X)$  is the complementary error function. It is important to note that these quantities are linear in  $c_0$  and do not depend on  $k_r$ . Thus, the ratio of  $N_{res}$  and the number of lipids in a bilayer is inversely proportional to  $L_X$  (and  $L_Y$ ), implying that the effects of V(X) on binary bilayers diminish in larger system. The restraining energy distribution along X = V(X)p(X) has a peak at  $2^{1/2}\sigma$  and the majority (95%) of the lipids (under  $V(X) < 2k_BT$ ) are distributed within  $2\sigma$  from  $X_0$ .

#### A2. Detailed description of the model for gA-lipid interactions in the BBS

Here, we describe a model for gA-lipid interactions in **Sec. V** in detail. In the model, it is assumed that  $G(X_{gA})$  includes the contributions up to the third lipid shell of a gA  $(R_3 \approx 30 \text{ Å from } X_{gA})$ . It is also assumed that the free energy comprises the contributions from the bilayer deformation ( $G_{def}$ ),

the line tension ( $G_{int}$ ), and the restraining potential ( $G_{res}$ ). Then, the PMF profile of gA in a BBS in a range of  $X_{gA}$ , [ $-L_X/4$ ,  $L_X/4$ ], is modeled as:

- 1)  $G_{\text{def}}$  is the contribution from the bilayer deformation energy far from the interfaces between bilayers. It is a constant ( $G_{\text{def}}$  (B1) and  $G_{\text{def}}$  (B2) in bilayers B1 and B2, respectively) when  $|X_{\text{gA}}| > R_3$ . The change of  $G_{\text{def}}$  from  $X_{\text{gA}} = -R_3$  to  $X_{\text{gA}} = R_3$  is assumed to be proportional to the number of gA-contacting lipids of B1 or B2,  $N_{\text{cont}}$ (B1) or  $N_{\text{cont}}$ (B2) and is simplified to be linear from one state to the other based on **Fig. 3C**;
- 2)  $G_{\text{int}}$  is the contribution from the energy due the line tension  $\gamma$  along the line segment L of the B1-B2 interface (i.e., along the Y direction) up to the third lipid shell of a gA ( $G_{\text{int}} = \gamma L$ ). The line segment L becomes 0 when  $|X_{\text{gA}}| > R_3$  and is simplified to decrease linearly from  $L = 2R_3$  to L = 0 as  $X_{\text{gA}}$  changes from 0 Å to  $\pm R_3$ ;
- 3)  $G_{\rm res}$  is the contribution from the energy due to the restrained lipids up to the third lipid shell. The restraining energy distribution from B1 (whose X center < 0) is simplified to be a uniform line density of  $\rho^{\rm B1} = E_{\rm res}^{\rm B1}/(2L_Y)$  at  $X = X_{\rm M} + 2^{1/2}\sigma$ . Then,  $G_{\rm res}$  from B1 can be approximately described as  $G_{\rm res}^{\rm B1} = \rho^{\rm B1}L^{\rm B1}$  where  $L^{\rm B1}$  is the line segment along the Y direction at  $X = X_{\rm M} + 2^{1/2}\sigma$  up to the third lipid shell of a gA. Therefore,  $L^{\rm B1}$  becomes 0 when  $|X_{\rm gA} (X_{\rm M} + 2^{1/2}\sigma)| > R_3$  and is simplified to decrease linearly from  $L^{\rm B1} = 2R_3$  to  $L^{\rm B1} = 0$  as  $X_{\rm gA}$  changes from  $X_{\rm M} + 2^{1/2}\sigma$  to  $X_{\rm M} + 2^{1/2}\sigma \pm R_3$ .  $G_{\rm res}^{\rm B2}$  can be modeled similarly.
- 4) Considering the geometry of the BBS and its periodic images, G has reflectional symmetry, whose lines of symmetry are  $X_{gA} = -L_X/4$  and  $X_{gA} = L_X/4$  (i.e., centers of each bilayer).

To calculate the model PMF profile for the present study, we used  $G_{\text{def}}(\text{DLPC}) = 2.17 \text{ kcal/mol}$  and  $G_{\text{def}}(\text{DMPC}) = 0.01 \text{ kcal/mol}$  (i.e.,  $\Delta G_{\text{def}} = -2.2 \text{ kcal/mol}$ ) from the CEM Eq. (3) (**Table 4**). The line tension  $\gamma$  at the DLPC/DMPC boundary is given by the equation<sup>74</sup>

$$\gamma = \frac{\sqrt{\kappa_C^{\text{B1}} \kappa_{\theta}^{\text{B1}} \kappa_C^{\text{B2}} \kappa_{\theta}^{\text{B2}}}}{\sqrt{\kappa_C^{\text{B1}} \kappa_{\theta}^{\text{B1}}} + \sqrt{\kappa_C^{\text{B2}} \kappa_{\theta}^{\text{B2}}}} \frac{\delta^2}{h_0^2}$$
(A3)

where B1 and B2 represent DLPC and DMPC bilayers,  $K_C$  and  $K_\theta$  are the bilayer bending and tilt moduli,  $\delta$  is the hydrophobic mismatch between B1 and B2, and  $h_0$  is the average hydrophobic thickness of B1 and B2. Note that the spontaneous curvatures of phosphatidylcholine bilayers are assumed to be negligible. Using the bending and tilt moduli  $K_C = 7.82 \times 10^{-20}$  J and  $K_\theta = 58.5$  mN/m for DLPC bilayers and  $K_C = 1.02 \times 10^{-19}$  J and  $K_\theta = 32.3$  mN/m for DMPC bilayers (at T = 303.15 K) (Venable, et al., in preparation), and the hydrophobic thicknesses from Ref. 66:  $d_H = 21.2$  Å and  $d_H = 25.3$  Å for DLPC and DMPC bilayers, respectively, the calculated line tension  $\gamma = 0.97$  pN. Lastly, using  $E_{\rm res}^{\rm DLPC} = 1.16$  kcal/mol,  $E_{\rm res}^{\rm DMPC} = 1.06$  kcal/mol, and  $E_{\rm res}^{\rm DMPC} = 1.06$  kcal/mol, and  $E_{\rm res}^{\rm DLPC} = 1.06$  kcal/mol as  $E_{\rm res}^{\rm DLPC} = 1.06$  kcal/mol.Å) and  $E_{\rm res}^{\rm DMPC} = 1.06 \times 10^{-3}$  kcal/(mol·Å), respectively.

#### **AUTHOR INFORMATION**

## **Corresponding Authors**

\*(W. I.) Tel: +1-610-758-4524. Fax: +1-610-758-4004. E-mail: wonpil@lehigh.edu.

\*(R. W. P.) Tel: +1-301-435-2035. Fax: +1-301-480-5496. E-mail: <u>pastorr@nhlbi.nih.gov</u>

#### **Notes**

The authors declare no competing financial interests.

#### **ACKNOWLEDGEMENTS**

This work was supported by NSF MCB-1727508, MCB-1810695, and XSEDE MCB070009 (to WI), the National Institute of Supercomputing and Networking/Korea Institute of Science and Technology Information, with supercomputing resources including technical support (KSC-2018-CRE-0068 to MSY), NIH R01-GM021342 (to OSA), and the Intramural Research Program of the National Institutes of Health, National Heart, Lung and Blood Institute, including the high performance computational capabilities of the NHLBI LoBoS cluster (to RWP).

#### REFERENCES

- (1) Andersen, O. S.; Koeppe, R. E. Bilayer Thickness and Membrane Protein Function: An Energetic Perspective. *Annu. Rev. Biophys. Biomol. Struct.* **2007**, *36*, 107–130.
- (2) Kim, T.; Im, W. Revisiting Hydrophobic Mismatch with Free Energy Simulation Studies of Transmembrane Helix Tilt and Rotation. *Biophys. J.* **2010**, *99* (1), 175–183.
- (3) Lundbæk, J. A.; Andersen, O. S.; Werge, T.; Nielsen, C. Cholesterol-Induced Protein Sorting: An Analysis of Energetic Feasibility. *Biophys. J.* **2003**, *84*, 2080–2089.
- (4) Mondal, S.; Khelashvili, G.; Shan, J.; Andersen, O. S.; Weinstein, H. Quantitative Modeling of Membrane Deformations by Multihelical Membrane Proteins: Application to G-Protein Coupled Receptors. *Biophys. J.* **2011**, *101*, 2092–2101.
- (5) Bransburg-Zabary, S.; Kessel, A.; Gutman, M.; Ben-Tal, N. Stability of an Ion Channel in Lipid Bilayers: Implicit Solvent Model Calculations with Gramicidin. *Biochemistry* **2002**, *41* (22), 6946–6954.
- (6) Yeh, I. C.; Olson, M. A.; Lee, M. S.; Wallqvist, A. Free-Energy Profiles of Membrane Insertion of the M2 Transmembrane Peptide from Influenza A Virus. *Biophys. J.* **2008**, *95* (11), 5021–5029.
- (7) Gumbart, J.; Chipot, C.; Schulten, K. Free-Energy Cost for Translocon-Assisted Insertion of Membrane Proteins. *Proc. Natl. Acad. Sci.* **2011**, *108* (9), 3596–3601.
- (8) Gumbart, J.; Roux, B. Determination of Membrane-Insertion Free Energies by Molecular Dynamics Simulations. *Biophys. J.* **2012**, *102* (4), 795–801.
- (9) Bereau, T.; Bennett, W. F. D.; Pfaendtner, J.; Deserno, M.; Karttunen, M. Folding and Insertion Thermodynamics of the Transmembrane WALP Peptide. *J. Chem. Phys.* **2015**, *143* (24), 243127.
- (10) Owicki, J. C.; McConnell, H. M. Theory of Protein-Lipid and Protein-Protein Interactions in Bilayer Membranes. *Proc. Natl. Acad. Sci. U. S. A.* **1979**, *76* (10), 4750–4754.
- (11) Lee, J.; Im, W. Transmembrane Helix Tilting: Insights from Calculating the Potential of Mean Force. *Phys. Rev. Lett.* **2008**, *100* (1), 18103.
- (12) Argudo, D.; Bethel, N. P.; Marcoline, F. V.; Wolgemuth, C. W.; Grabe, M. New Continuum Approaches for Determining Protein-Induced Membrane Deformations. *Biophys. J.* **2017**, *112* (10), 2159–2172.
- (13) Park, S.; Im, W. Quantitative Characterization of Cholesterol Partitioning between Binary Bilayers. *J. Chem. Theory Comput.* **2018**, *14* (6), 2829–2833.
- (14) Sugita, Y.; Kitao, A.; Okamoto, Y. Multidimensional Replica-Exchange Method for Free-Energy Calculations. *J. Chem. Phys.* **2000**, *113* (15), 6042–6051.
- (15) Urry, D. W.; Prasad, K. U.; Trapane, T. L. Location of Monovalent Cation Binding Sites in the Gramicidin Channel. *Proc. Natl. Acad. Sci. U. S. A.* **1982**, *79* (2), 390–394.
- (16) Andersen, O. S. Gramicidin Channels. Annu. Rev. Physiol. 1984, 46, 531–548.
- (17) Antoinette Killian, J. Gramicidin and Gramicidin-Lipid Interactions. *BBA Rev. Biomembr.* **1992**, *1113* (3–4), 391–425.

- (18) Kelkar, D. A.; Chattopadhyay, A. The Gramicidin Ion Channel: A Model Membrane Protein. *Biochim. Biophys. Acta Biomembr.* **2007**, *1768*, 2011–2025.
- (19) Wallace, B. A. Common Structural Features in Gramicidin and Other Ion Channels. *BioEssays* **2000**, *22* (3), 227–234.
- (20) Valiyaveetil, F. I.; Sekedat, M.; MacKinnon, R.; Muir, T. W. Glycine as a D-Amino Acid Surrogate in the K+-Selectivity Filter. *Proc. Natl. Acad. Sci.* **2004**, *101* (49), 17045–17049.
- (21) Wimley, W. C.; White, S. H. Experimentally Determined Hydrophobicity Scale for Proteins at Membrane Interfaces. *Nat. Struct. Biol.* **1996**, *3*, 842–848.
- (22) Domene, C.; Vemparala, S.; Klein, M. L.; Vénien-Bryan, C.; Doyle, D. A. Role of Aromatic Localization in the Gating Process of a Potassium Channel. *Biophys. J.* **2006**, *90* (1), L01–L03.
- (23) Harroun, T. A.; Heller, W. T.; Weiss, T. M.; Yang, L.; Huang, H. W. Experimental Evidence for Hydrophobic Matching and Membrane- Mediated Interactions in Lipid Bilayers Containing Gramicidin. *Biophys. J.* **1999**, *76* (2), 937–945.
- (24) Beaven, A. H.; Sodt, A. J.; Pastor, R. W.; Koeppe, R. E.; Andersen, O. S.; Im, W. Characterizing Residue-Bilayer Interactions Using Gramicidin A as a Scaffold and Tryptophan Substitutions as Probes. *J. Chem. Theory Comput.* **2017**, *13* (10), 5054–5064.
- (25) Lee, K. I.; Pastor, R. W.; Andersen, O. S.; Im, W. Assessing Smectic Liquid-Crystal Continuum Models for Elastic Bilayer Deformations. *Chem. Phys. Lipids* **2013**, *169*, 19–26.
- (26) Sodt, A. J.; Beaven, A. H.; Andersen, O. S.; Im, W.; Pastor, R. W. Gramicidin A Channel Formation Induces Local Lipid Redistribution II: A 3D Continuum Elastic Model. *Biophys. J.* **2017**, *112* (6), 1198–1213.
- (27) Huang, H. W. Deformation Free Energy of Bilayer Membrane and Its Effect on Gramicidin Channel Lifetime. *Biophys. J.* **1986**, *50* (6), 1061–1070.
- (28) Helfrich, P.; Jakobsson, E. Calculation of Deformation Energies and Conformations in Lipid Membranes Containing Gramicidin Channels. *Biophys. J.* **1990**, *57* (5), 1075–1084.
- (29) Lundbæk, J. A.; Collingwood, S. A.; Ingólfsson, H. I.; Kapoor, R.; Andersen, O. S. Lipid Bilayer Regulation of Membrane Protein Function: Gramicidin Channels as Molecular Force Probes. *J. R. Soc. Interface* **2010**, *7*, 373–395.
- (30) Kim, T.; Lee, K. I.; Morris, P.; Pastor, R. W.; Andersen, O. S.; Im, W. Influence of Hydrophobic Mismatch on Structures and Dynamics of Gramicidin A and Lipid Bilayers. *Biophys. J.* **2012**, *102* (7), 1551–1560.
- (31) Beaven, A. H.; Maer, A. M.; Sodt, A. J.; Rui, H.; Pastor, R. W.; Andersen, O. S.; Im, W. Gramicidin A Channel Formation Induces Local Lipid Redistribution I: Experiment and Simulation. *Biophys. J.* **2017**, *112* (6), 1185–1197.
- (32) Elliott, J. R.; Needham, D.; Dilger, J. P.; Haydon, D. A. The Effects of Bilayer Thickness and Tension on Gramicidin Single-Channel Lifetime. *Biochim. Biophys. Acta, Biomembr.* **1983**, *735* (1), 95–103.

- (33) Townsley, L. E.; Tucker, W. A.; Sham, S.; Hinton, J. F. Structures of Gramicidins A, B, and C Incorporated into Sodium Dodecyl Sulfate Micelles. *Biochemistry* **2001**, *40* (39), 11676–11686.
- (34) Park, S.; Kim, T.; Im, W. Transmembrane Helix Assembly by Window Exchange Umbrella Sampling. *Phys. Rev. Lett.* **2012**, *108* (10), 108102.
- (35) Jo, S.; Kim, T.; Iyer, V. G.; Im, W. CHARMM-GUI: A Web-Based Graphical User Interface for CHARMM. *J. Comput. Chem.* **2008**, *29* (11), 1859–1865.
- (36) Jo, S.; Kim, T.; Im, W. Automated Builder and Database of Protein/Membrane Complexes for Molecular Dynamics Simulations. *PLoS One* **2007**, *2* (9), e880.
- (37) Jo, S.; Lim, J. B.; Klauda, J. B.; Im, W. CHARMM-GUI Membrane Builder for Mixed Bilayers and Its Application to Yeast Membranes. *Biophys. J.* **2009**, *97* (1), 50–58.
- (38) Wu, E. L.; Cheng, X.; Jo, S.; Rui, H.; Song, K. C.; Davila-Contreras, E. M.; Qi, Y. F.; Lee, J. M.; Monje-Galvan, V.; Venable, R. M.; et al. CHARMM-GUI Membrane Builder Toward Realistic Biological Membrane Simulations. *J. Comp. Chem.* **2014**, *35* (27), 1997–2004.
- (39) Yoo, J.; Cui, Q. Three-Dimensional Stress Field around a Membrane Protein: Atomistic and Coarse-Grained Simulation Analysis of Gramicidin A. *Biophys. J.* **2013**, *104* (1), 117–127.
- (40) Yoo, J.; Cui, Q. Membrane-Mediated Protein-Protein Interactions and Connection to Elastic Models: A Coarse-Grained Simulation Analysis of Gramicidin A Association. *Biophys. J.* **2013**, *104* (1), 129–138.
- (41) Nielsen, C.; Goulian, M.; Andersen, O. S. Energetics of Inclusion-Induced Bilayer Deformations. *Biophys. J.* **1998**, *74* (4), 1966–1983.
- (42) Nielsen, C.; Andersen, O. S. Inclusion-Induced Bilayer Deformations: Effects of Monolayer Equilibrium Curvature. *Biophys. J.* **2000**, *79* (5), 2583–2604.
- (43) Partenskii, M. B.; Jordan, P. C. Membrane Deformation and the Elastic Energy of Insertion: Perturbation of Membrane Elastic Constants Due to Peptide Insertion. *J. Chem. Phys.* **2002**, *117*, 10768.
- (44) Eastman, P.; Swails, J.; Chodera, J. D.; McGibbon, R. T.; Zhao, Y. T.; Beauchamp, K. A.; Wang, L. P.; Simmonett, A. C.; Harrigan, M. P.; Stern, C. D.; et al. OpenMM 7: Rapid Development of High Performance Algorithms for Molecular Dynamics. *PloS Comput. Biol.* **2017**, *13* (7).
- (45) Huang, J.; Mackerell, A. D. CHARMM36 All-Atom Additive Protein Force Field: Validation Based on Comparison to NMR Data. *J. Comput. Chem.* **2013**, *34* (25), 2135–2145.
- (46) Klauda, J. B.; Venable, R. M.; Freites, J. A.; O'Connor, J. W.; Tobias, D. J.; Mondragon-Ramirez, C.; Vorobyov, I.; MacKerell, A. D.; Pastor, R. W. Update of the CHARMM All-Atom Additive Force Field for Lipids: Validation on Six Lipid Types. *J. Phys. Chem. B* **2010**, *114* (23), 7830–7843.

- (47) Jorgensen, W. L.; Chandrasekhar, J.; Madura, J. D.; Impey, R. W.; Klein, M. L. Comparison of Simple Potential Functions for Simulating Liquid Water. *J. Chem. Phys.* **1983**, *79* (2), 926–935.
- (48) Durell, S. R.; Brooks, B. R.; Bennaim, A. Solvent-Induced Forces between Two Hydrophilic Groups. *J. Phys. Chem.* **1994**, *98* (8), 2198–2202.
- (49) Neria, E.; Fischer, S.; Karplus, M. Simulation of Activation Free Energies in Molecular Systems. *J. Chem. Phys.* **1996**, *105* (5), 1902–1921.
- (50) Ryckaert, J.-P.; Ciccotti, G.; Berendsen, H. J. C. Numerical Integration of the Cartesian Equations of Motion of a System with Constraints: Molecular Dynamics of n-Alkanes. *J. Comput. Phys.* **1977**, *23* (3), 327–341.
- (51) Steinbach, P. J.; Brooks, B. R. New Spherical-Cutoff Methods for Long-Range Forces in Macromolecular Simulation. *J. Comput. Chem.* **1994**, *15* (7), 667–683.
- (52) Essmann, U.; Perera, L.; Berkowitz, M. L.; Darden, T.; Lee, H.; Pedersen, L. G. A Smooth Particle Mesh Ewald Method. *J. Chem. Phys.* **1995**, *103* (19), 8577–8593.
- (53) Chow, K. H.; Ferguson, D. M. Isothermal-Isobaric Molecular Dynamics Simulations with Monte Carlo Volume Sampling. *Comput. Phys. Commun.* **1995**, *91* (1–3), 283–289.
- (54) Åqvist, J.; Wennerström, P.; Nervall, M.; Bjelic, S.; Brandsdal, B. O. Molecular Dynamics Simulations of Water and Biomolecules Wit a Monte Carlo Constant Pressure Algorithm. *Chem. Phys. Lett.* **2004**, *384* (4–6), 288–294.
- (55) Lee, J.; Cheng, X.; Swails, J. M.; Yeom, M. S.; Eastman, P. K.; Lemkul, J. A.; Wei, S.; Buckner, J.; Jeong, J. C.; Qi, Y.; et al. CHARMM-GUI Input Generator for NAMD, GROMACS, AMBER, OpenMM, and CHARMM/OpenMM Simulations Using the CHARMM36 Additive Force Field. *J. Chem. Theory Comput.* **2016**, *12* (1), 405–413.
- (56) Pandit, S. A.; Vasudevan, S.; Chiu, S. W.; Mashl, R. J.; Jakobsson, E.; Scott, H. L. Sphingomyelin-Cholesterol Domains in Phospholipid Membranes: Atomistic Simulation. *Biophys. J.* **2004**, *87* (2), 1092–1100.
- (57) Kim, T.; Jo, S.; Im, W. Solid-State NMR Ensemble Dynamics as a Mediator between Experiment and Simulation. *Biophys. J.* **2011**, *100* (12), 2922–2928.
- (58) Killian, J. A.; Prasad, K. U.; Hains, D.; Urry, D. W. The Membrane as an Environment of Minimal Interconversion: A Circular Dichroism Study on the Solvent Dependence of the Conformational Behavior of Gramicidin in Diacylphosphatidylcholine Model Membranes. *Biochemistry* 1988, 27 (13), 4848–4855.
- (59) Benz, R.; Fröhlich, O.; Läuger, P.; Montal, M. Electrical Capacity of Black Lipid Films and of Lipid Bilayers Made from Monolayers. *BBA Biomembr.* **1975**, *394* (3), 323–334.
- (60) Kolb, H. A.; Bamberg, E. Influence of Membrane Thickness and Ion Concentration on the Properties of the Gramicidin A Channel. Autocorrelation, Spectral Power Density, Relaxation and Single-Channel Studies. *BBA Biomembr.* **1977**, *464* (1), 127–141.
- (61) Woolf, T. B.; Roux, B. Structure, Energetics, and Dynamics of Lipid-Protein Interactions: A Molecular Dynamics Study of the Gramicidin A Channel in a DMPC Bilayer. *Proteins Struct. Funct. Genet.* **1996**, *24* (1), 92–114.

- (62) Chiu, S. W.; Subramaniam, S.; Jakobsson, E. Simulation Study of a Gramicidin/Lipid Bilayer System in Excess Water and Lipid. I. Structure of the Molecular Complex. *Biophys. J.* **1999**, *76* (4), 1929–1938.
- (63) Rice, D.; Oldfield, E. Deuterium Nuclear Magnetic Resonance Studies of the Interaction between Dimyristoylphosphatidylcholine and Gramicidin A'. *Biochemistry* **1979**, *18* (15), 3272–3279.
- (64) Perly, B.; Smith, I. C. P.; Jarrell, H. C. Acyl Chain Dynamics of Phosphatidylethanolamines Containing Oleic Acid and Dihydrosterculic Acid: 2H NMR Relaxation Studies. *Biochemistry* **1985**, *24* (17), 4659–4665.
- (65) Douliez, J. P.; Léonard, A.; Dufourc, E. J. Restatement of Order Parameters in Biomembranes: Calculation of C-C Bond Order Parameters from C-D Quadrupolar Splittings. *Biophys. J.* **1995**, *68* (5), 1727–1739.
- (66) Zhuang, X.; Dávila-Contreras, E. M.; Beaven, A. H.; Im, W.; Klauda, J. B. An Extensive Simulation Study of Lipid Bilayer Properties with Different Head Groups, Acyl Chain Lengths, and Chain Saturations. *Biochim. Biophys. Acta Biomembr.* **2016**, *1858* (12), 3093–3104.
- (67) Lundbæk, J. A.; Andersen, O. S. Spring Constants for Channel-Induced Lipid Bilayer Deformations Estimates Using Gramicidin Channels. *Biophys. J.* **1999**, *76*, 889–895.
- (68) Rawicz, W.; Olbrich, K. C.; McIntosh, T.; Needham, D.; Evans, E. Effect of Chain Length and Unsaturation on Elasticity of Lipid Bilayers. *Biophys. J.* **2000**, *79* (1), 328–339.
- (69) Kučerka, N.; Nieh, M. P.; Katsaras, J. Fluid Phase Lipid Areas and Bilayer Thicknesses of Commonly Used Phosphatidylcholines as a Function of Temperature. *Biochim. Biophys. Acta-Biomembranes* **2011**, *1808* (11), 2761–2771.
- (70) Lewis, B. A.; Engelman, D. M. Lipid Bilayer Thickness Varies Linearly with Acyl Chain Length in Fluid Phosphatidylcholine Vesicles. *J. Mol. Biol.* **1983**, *15* (166), 211–217.
- (71) Nagle, J. F.; Zhang, R.; Tristram-Nagle, S.; Sun, W.; Petrache, H. I.; Suter, R. M. X-Ray Structure Determination of Fully Hydrated Lα Phase Dipalmitoylphosphatidylcholine Bilayers. *Biophys. J.* **1996**, *70* (3), 1419–1431.
- (72) Venable, R. M.; Brown, F. L. H.; Pastor, R. W. Mechanical Properties of Lipid Bilayers from Molecular Dynamics Simulation. *Chem. Phys. Lipids* **2015**, *192*, 60–74.
- (73) Fattal, D. R.; Ben-Shaul, A. A Molecular Model for Lipid-Protein Interaction in Membranes: The Role of Hydrophobic Mismatch. *Biophys. J.* **1993**, *65*, 1795–1809.
- (74) Kuzmin, P. I.; Akimov, S. A.; Chizmadzhev, Y. A.; Zimmerberg, J.; Cohen, F. S. Line Tension and Interaction Energies of Membrane Rafts Calculated from Lipid Splay and Tilt. *Biophys. J.* **2005**, *88* (2), 1120–1133.

# For Table of Contents Only

